Gecko-inspired dry adhesives for heritage conservation – tackling the surface roughness with empirical testing and finite element modelling

Jacek Olender, Jack Perris, Yang Xu, Christina Young, Daniel M. Mulvihill & Nikolaj Gadegaard

Taylor & Francis
Taylor & Francis Group

Gecko-inspired dry adhesives for heritage conservation – tackling the surface roughness with empirical testing and finite element modelling

Jacek Olender[a], Jack Perris[b], Yang Xu[c], Christina Young[a], Daniel M. Mulvihill[b] and Nikolaj Gadegaard[b]

[a]Kelvin Centre for Conservation and Cultural Heritage Research, School of Culture and Creative Arts, University of Glasgow, Glasgow, UK; [b]James Watt School of Engineering, University of Glasgow, Glasgow, UK; [c]School of Mechanical Engineering, Hefei University of Technology, Hefei, China

ABSTRACT

Gecko-inspired dry adhesives (GDAs) have been developed in an attempt to replicate in polymer material the natural ability of some gecko lizards to attach to nearly any surface. Geckos achieve this with nano-sized structures on their feet that facilitate van der Waals's interactions with the surfaces. The conservation of cultural heritage is an area that could benefit greatly from the introduction of a versatile and easily reversible adhesive. However, the multitude of surface types and various surface textures encountered in this field make the adaptation of GDAs difficult. In this research two types of GDAs, with flat tips and with mushroom-shaped tips have been assessed using pull-off tests on three substrate materials. These are based on real heritage objects' surfaces (copper and ceramic) with different levels of surface roughness from The Hunterian collection. Adhesive strength varied between different GDAs and as expected adhesive strength reduced with increased substrate roughness. The finite Element Modelling (FEM) of the pull-off tests closely matched empirical results and showed how different behaviours on the microlevel can affect the GDA behaviour on rough surfaces. It helped to understand the microscale behaviour of two different types of GDAs tested. The research has shown the necessary direction for experimental and theoretical research on GDAs which will enable them to be adopted more widely in heritage conservation.

1. Introduction

Geckos are a group of lizards known for having the ability to stick to nearly any surface they move on, regardless of the angle between that surface and the ground [1]. This ability

has inspired the development of gecko-like adhesives, commonly known as gecko-inspired dry adhesives (GDAs) [2,3]. GDAs have become a focus for heritage conservation because of their relatively strong normal and shear adhesion (comparable with some pressure-sensitive adhesive tapes), combined with very low peel strength. These properties are sought after in a number of heritage conservation applications, where such strong adhesion and easy removal ability are required [4–6]. This aligns with one of the key principles of heritage conservation, i.e. the reversibility of intervention to the structure of the heritage object [7–10]. That is why the very low peel of GDAs, while a disadvantage in most industries has a great potential for heritage conservation, where object handling is very careful at all times. Despite some early successes in applications of GDAs for conservation purposes as adhesives [5,11,12], or as cleaning agents [13], research to date has confirmed our assumptions that certain materials with weathered and heavily abraded surfaces are not suitable for GDAs attachment. Thus, this research is aimed at establishing the range of roughness for using GDAs on surfaces that are commonly found in mixed museum collections as well as understanding the behaviour of currently available GDAs. The variety of materials and surface qualities among the objects in museum collections is virtually boundless. Even the surfaces that are, in principle, working very well with GDAs, for example, glass or ceramics, have been shown to lose that capability with increased surface roughness [4,5]. This requires quantification if new adhesives for the surfaces commonly found in heritage objects are to be designed. FEM was essential in understanding differences in behaviour between two different types of GDAs used in this research – one with mushroom caps on the tips of its micropillars and one with flat punch tips.

Geckos in nature can cope with a wide range of roughness and it had been assumed at one point that gecko-inspired adhesives might be applicable to rough surfaces typically found in heritage conservation [14]. But it has been shown that the range of surface roughness, in which asperities on the surface are similar in size to the size of a single gecko spatula, lowers the adhesion in live gecko lizards, by up to 50% [15–17]. Yet in the wild some multi-habitat gecko species have been found to actively prefer walking on rougher surfaces over smoother ones, up to 80% of the time [18], meaning that having two surfaces to walk on with different roughness, they would actively choose a path over the rougher one. As Pillai et al. suggest, this is caused by the animal's better clinging performance on rougher surfaces. However, at present artificial gecko adhesion has not yet reached the versatility of natural gecko adhesion [19–21]. And although the influence of roughness on fibrillar adhesion has been studied in both natural and artificial gecko adhesion, there are still gaps in the understanding of this area [22]. Surfaces investigated in gecko adhesion research to date include glass, either flat [23,24] or spherical [25], ceramic tiles [26], ruby [27], PVS [28], silicon wafers and sandpapers [17]. Fischer et al. [29] and Kasem and Varenberg [30] made epoxy moulds of everyday materials in order to investigate the roughness and other features of surface metrology, while making sure that other properties of these surfaces, for example, electrostaticity or surface energy, stay constant. However, Fischer et al. [29] reported differences in roughness between the moulded epoxy surfaces and the originals. In some research rough surfaces are tested with a GDA, but their roughness is not reported [31].

Published research on the relationship between artificial gecko adhesion and roughness most commonly reports Rq (Root Mean Square, RMS) and Ra (arithmetical mean

deviation, Raa) as roughness parameters used in the analysis [17,28]. However, some publications include more complex parameters, available with modern profilometers and software, for instance, profile skewness and profile kurtosis or maximum height of the profile [25,26,32]. Furthermore, Kasem and Varenberg [30] have shown that Ra is not a reliable parameter for predicting the strength of adhesion in fibrillar adhesives, nor did they find any significant correlation with any other single parameter describing roughness. Instead, they have proposed introducing a new parameter 'Ri', which is based on the relative height and diameter of asperities on the surface and which fitted their experimental measurements better than Ra. The most commonly reported roughness measurement techniques are white light interferometry [17,28,33], stylus profilometry [24,29], confocal microscopy [27], and atomic force microscopy (AFM) [25,34].

There has been some testing done with multiple GDAs on surfaces with varying roughness, using tensile, pull-off and shear adhesion to evaluate the materials' performance. Ruffatto et al. [26] tested four different types of GDAs in shear on ceramic tiles with various grades of roughness as well as several man-made surfaces, comparing them with natural gecko adhesion. They aimed to demonstrate the advantages that their new hybrid, the electrostatic adhesive had over non-electrified adhesives. Cañas et al. [17] tested smooth PDMS and micropatterned PDMS on nano- and micro-rough surfaces. They found that the adhesion of micropatterned PDMS exceeded the adhesion of unpatterned PDMS on rougher surfaces, probably due to better inhibition of the crack initiation phenomena occurring at the edges of the square silica probes. They showed that micropatterned PDMS adheres best to surfaces with asperities of similar size to the surface pattern. This result suggests that micropatterned PDMS behaves differently from the natural gecko adhesive pads, which adhere the least to surfaces with asperities of the size similar to the gecko spatulae [15]. Barreau et al. [24] tested cylindrical-patterned PDMS GDAs on glass substrates with pull-off tests. They tested three different GDAs, with different micropillar diameters on three glass substrates with varying roughness. The GDAs achieved a very high pull-off stress (in the range of several kPa), from small samples (8×8 mm). However, it should be noted that GDA adhesion has significant issues with scalability and the results achieved on samples with several mm^2 do not linearly increase with the increase of the sample area [5,22].

In the field of heritage conservation, the term 'roughness' often has a generic meaning, comparing 'smooth' versus 'rough' surfaces in a single object or between two similar objects [35]. In many cases, the term 'a rough surface' refers to a surface deteriorated by environmental conditions or biological action. The rough surface is compared to the smoother parts, which are in a better state of preservation [36–38]. Similarly, other authors use the term 'rough' as an adjective describing the property of surface texture and understood as an aesthetic effect left by the artist [39,40]. The term is also used to mark local wear or degradation, but it also is used for comparison between the state of the surface before and after treatment [41,42]. Stylus profilometry and confocal microscopy are the most common roughness measurement methods [41–46]. For the purpose of examining surfaces of the original heritage objects, the most useful in this context profilometers are those that allow complete objects to be tested, like optical and mechanical profilometers. However, the latter poses a risk for heritage objects, as they might scratch the object's surface, a significant issue in heritage

preservation. Optical profilometers offer good vertical resolution and reasonable horizontal resolution while scanning fast over larger areas without touching the object. White light interferometry, optical microscopy with multi focus stacking and AFM also have been occasionally used [47–49]. Such stacking optical microscopy allows depth maps to be created, from which extraction of surface parameters is possible [47,50]. Less precise methods are also described, for example, pixel analysis of digital greyscale photographs of surfaces under raking light [46]. In conservation research, the most popular roughness parameter used is Rq (RMS, root mean square), followed by Ra [45,46]. In recent years three-dimensional surface metrology together with surface profiling (using Sa and Sq parameters) have been preferred over linear profilometry [41,47,48,50].

To the authors' knowledge, there has not been a detailed explanation of behaviour of individual micropillars on the surfaces discussed in this paper. This is a necessary foundation for designing new GDAs for surfaces present in museum collections. Before the development of an appropriate FE model a review of adhesion mechanisms and modelling seen in contact mechanics problems as well as the existing FE implementations within the field of gecko-inspired dry adhesives was necessary. It is known that shape optimisation of a GDA's pillars can significantly increase the performance of adhesion and that mushroom-tip structured pillars are generally the shape noted for increasing performance [51]. There are limited examples of FE simulations of pillars in a GDA, but many of the ones performed have a focus on shape optimisation. Initial FE simulations have previously been developed based on adhesion behaviour [52–54]. Carbone et al. extensively investigated the shape optimisation and consequential separation mechanisms experienced by the GDA pillars [51–53]. They varied the geometry of both mushroom tip and cylindrical tip to see how this would influence the detachment mechanisms. The two tips were chosen based on their availability and significant difference in geometry between them. Using simplified FE modelling they simulated the pull-off mechanism that would occur and by extension implemented this data in the optimisation of the adhesion force exhibited by the pillars. Li et al. [55] explored the influence of the shape of the GDA pillar, examining the effect of the head shape on the adhesion capability of the structure. They found that the adhesion effect improves with a smaller shaft radius and thinner mushroom head for connection to the substrate [55]. While Kim et al. developed an optimised free-form shape for the GDA pillars [56]. They utilised a deep learning-based optimisation using a neural network to perform an evaluation of the relationship between the shape of a pillar and its detachment mechanism and associated forces based on the interfacial stress distribution. Two pillar shapes were developed in this study that resemble previous design iterations, but are unique in their own right – one with a mushroom cap and on the flat-punch cylinder.

These studies are important examples of FE modelling of the gecko-inspired dry adhesives at the single-pillar level, and of how the shape of the pillars can influence the adhesion forces associated with a single pillar. The aim of our model is not, as of yet, to optimise the shape but to simulate the experimental configuration of the pull-off tests conducted in this research and described below. The design and implementation of the FE models developed for this study are described in the discussion, where the differences in the behaviour of the two types of GDAs are discussed. FE modelling was

also used to understand the behaviour of individual fibres on the tested surfaces (see Section 2.4).

It is hard to fully determine the possible performance of GDAs in heritage conservation applications without a more detailed experimental study and without understanding the behaviour of the GDAs on a single fibre level. Testing samples were prepared to represent real examples of heritage objects from museum collections, following their laboratory characterisation. Adhesion between three different materials from three different groups (ceramics, metals, and hydrophobic polymers) with various levels of surface abrasion and two types of GDAs, one with and one without mushroom caps on their fibres, were investigated in pull-off tests for macroscale adhesion. The selection of surfaces for the tests was determined based on discussions with the practising museum staff: conservators, collection managers, curators, and technicians. Actual heritage objects were examined and then substrates for adhesive testing were prepared based

2. Materials and methods

2.1. Sample acquisition and preparation

Heritage objects tested as references were either obtained from authors' own collections or from the collections of The Hunterian, University of Glasgow, UK. Several fragments of archaeological ceramics from both museum and private collections were investigated for potential examination as reference samples. Three pieces of glazed porcelain with various degrees of surface abrasion, one piece of non-glazed stoneware and one piece of glass were examined as well as two 19th century Victorian copper coins. These were two one-penny coins from 1865 and 1882 in two very different states of preservation – the former very smooth, with relief details barely visible and the latter with a very rough surface (Figure 1).

The two types of gecko adhesives used were: (1) a commercial GDA manufactured by the Gottlieb Binder GmbH (referred to below as: GB GDA), which has mushroom caps on its pillars and (2) a prototype GDA prepared at the University of Glasgow (referred to as: UOG GDA), which had straight, flat-tipped pillars on its adhesive surface (Figure 2). Substrate samples were prepared from stainless steel (type 304), a glazed ceramic tile, and a PTFE plate.

All materials for substrate samples were acquired from standard commercial suppliers (see list below). Glazed ceramic tiles, 100×300 mm each, were cut into 50×50 mm, ±1 mm squares. Steel samples were prepared from a 1 m long stainless steel square bar, with 50 mm, ±0.5 mm sides, and was cut into 5 mm, ±0.5 mm thick squares. The squares were milled on one side for greater uniformity before polishing. PTFE samples were prepared from a rectangular sheet of PTFE, 300×600 mm, 5 mm thick, and cut into 50×50 mm, ±1 mm squares using a utility knife. After cutting all samples were wet polished on a laboratory grinder (Struers LaboForce 50), at 200 rpm, with various grades of sandpapers (P120-P1200) or with silica polishing paste (Struers OP-U, 0.04 μm), in order to achieve various grades of roughness. Where higher values of roughness were needed samples were first polished to flatten the surface and subsequently were manually filed with a rough grade file. To achieve intermediate grades of
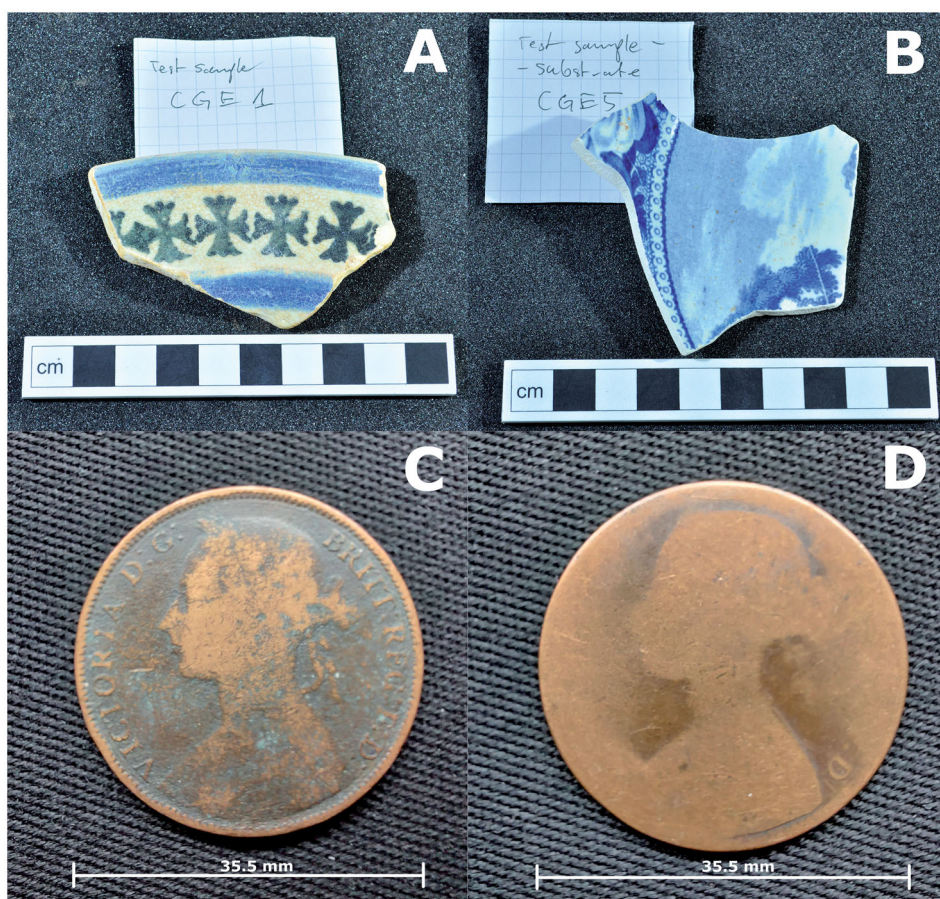
Figure 1. Examples of reference heritage objects: (A) CGE1 sample, a formerly glazed ceramic shard that had lost its glaze; (B) CGE5 sample, still glazed ceramic shard; (C) MCC1 sample (obverse) a rough-surfaced copper coin; (D) MCC2 sample, a smooth copper coin.

roughness some samples were delicately repolished on the grinder after filing. Samples of the GDAs were either bought from the manufacturer, Gottlieb Binder GmbH via their UK representative (the GB GDA) or manufactured locally (the UOG GDA). The commercially available GDA was acquired in a 100 mm wide stripe and the GDA manufactured locally was provided in circular moulds, 150 mm in diameter.

2.2. Sample characterisation – profilometry and surface energy

All samples were characterised with optical microscopy, optical and mechanical profilometry, and contact angle measurements to calculate their surface energy. For the purpose of optical profilometry, substrates were cleaned with acetone and ethanol immediately before the measurement. Each sample was scanned on the Alicona InfiniteFocus 4G 3D optical profilometer with a 10× magnification objective. Each sample was scanned two times, creating two perpendicular digital scans that allowed
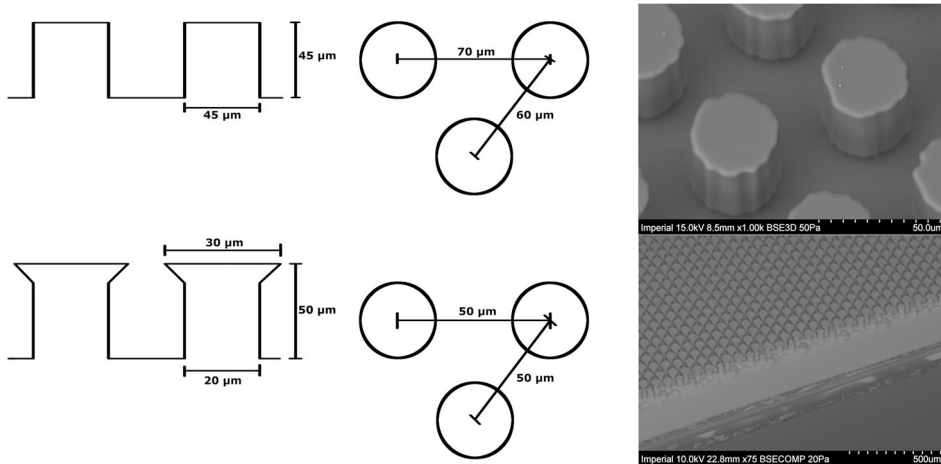
Figure 2. Schematic drawing with dimensions and ESEM images of the micropillars from both types of GDAs: UOG GDA (upper) and GB GDA (lower).
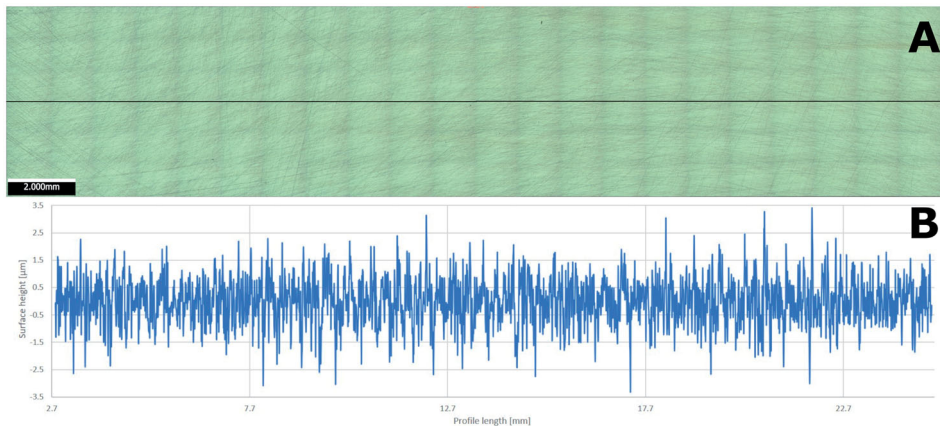
Figure 3. Example of a stitched scan of a substrate surface made with the optical profilometer with the extracted profile line (A) and the extracted profile (B).

for the extraction of surface profiles that were at least 15 mm long and allowed extraction of at least three profiles, 2 mm apart from each other. Both scans crossed the centre of the sample and were perpendicular to each other, being parallel with the edges of the sample. An example of such a profile extracted from the optical profilometer measurement is shown in Figure 3. As a result, each sample had six roughness profiles measured, in two perpendicular directions. Measurements were repeated with a mechanical stylus profilometer. The smoothest sample in each material category had to be measured exclusively with the mechanical profilometer (Mitutoyo SJ-210, with a round stylus tip with 0.75 mN of pressure and 0.002 mm diameter), because of excessive specular reflection of light that prevented taking effective measurements with the optical profilometer. The museum objects could not be transported outside of the museum and therefore could not be characterised with the optical profilometer, they

Figure 4. GDA samples adhered to the aluminium cubes. UOG GDA on the left and GB GDA on the right.

were examined using the stylus profilometer. The roughness values shown are the mean averages of values extracted from all profiles extracted from each sample.
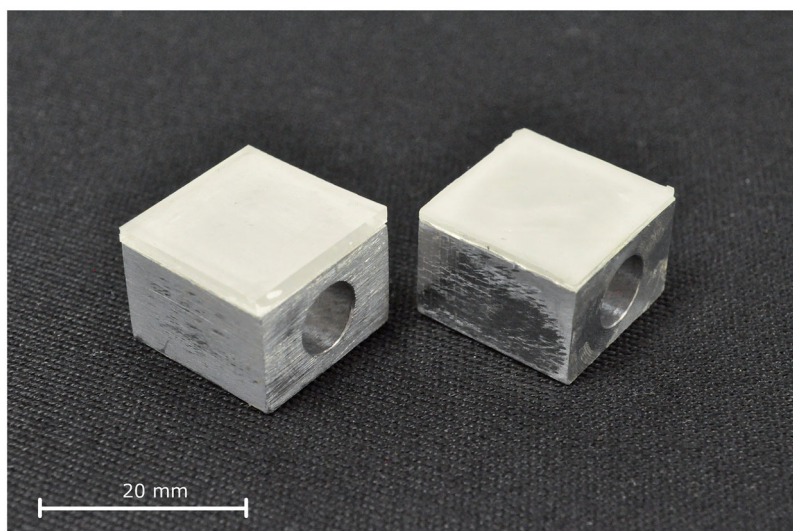
The surface energy of substrate surfaces and GDA polymers was calculated from sessile drop contact angle measurements. The contact angle kit was built in-house in accordance with the ISO standard [57], using a JAI GO-5000M-USB camera. Each surface was tested using four solvents: deionised water, xylene, ethylene glycol, and ethanol, each having different overall surface energy and different proportion of its polar and dispersive components.[1]

The same solvents were used on the PDMS of the GDAs, but without xylene, which is known to swell PDMS [60]. Each of the solvents was applied five times on each surface. Images of the drops were captured at 2 frames per second. The images for contact angle measurement taken at the 0.5–1 s interval from the droplet being placed on the surface were used to measure the contact angle. Images were processed in the ImageJ software suite with the Contact Angle plugin [61,62]. The average angle from all five drops was used in the surface energy calculations that were based on the Owens, Wendt, Rable and Kaelbe (OWRK) method [63–65].

2.3. Adhesion testing

The pull-off samples 20×20 mm squares of GDAs were cut out of the sheets of raw materials with a razor. Aluminium cubes were glued with Araldite Standard Ultra epoxy resin to the backs of the squares of GDAs. Cubes had dimensions of $\sim 19.5 \times 19.5 \times 10$ mm (width $\times$ length $\times$ height) and were drilled centrally, horizontally along their width. After mounting on a cube with the resin and after a bonding period of 24 h excess of the GDA was shaved off with a razor, adjusting the sample size to the size of each individual cube, as the cubes were not all identical. Examples can be seen in Figure 4. The maximum projected area of each sample available for contact was
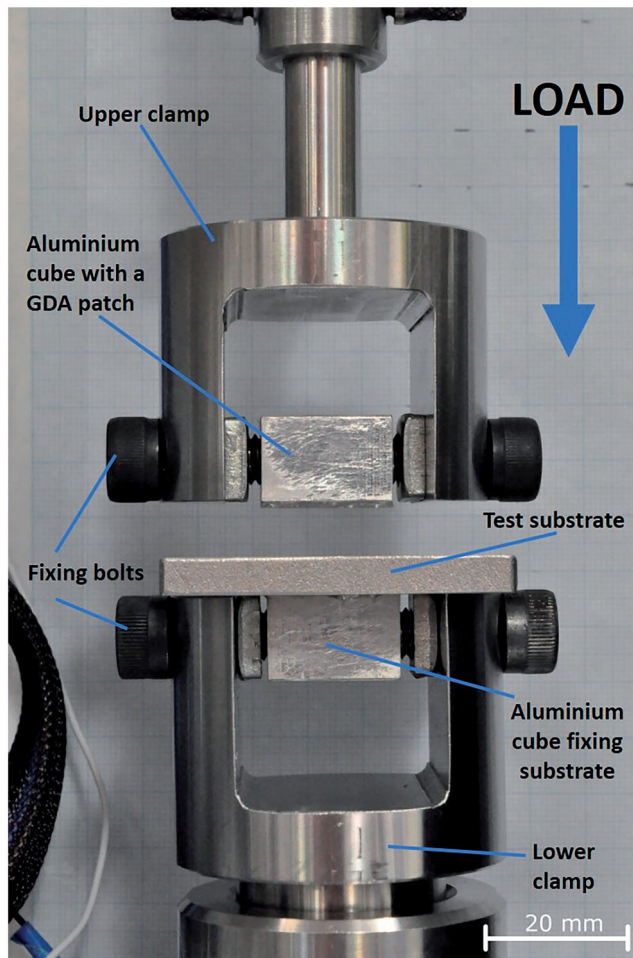
Figure 5. Pull-off testing setup. The substrates were placed in the bottom clamp and the GDAs were pressed onto them from the top.

$\sim$3.8 cm^2. Identical aluminium cubes with a hole drilled through the sides were glued to the centre of the back of each substrate sample using the same transparent Araldite epoxy resin. Environmental conditions in the laboratory during the final sample preparation were maintained at 20 °C, ±1 °C and 55% RH, ±5%. Cubes were used to mount both GDAs and substrate samples in the tensile tester, with the mount on the upper side allowing for 360° pivoting around the bolt, along the cube's width and $\sim$2° of pivoting freedom on the substrate, bottom side of the setup (Figure 5). The samples were suspended on bolts in custom-made stainless steel mounting jaws in such a way that the bolts holding the upper and the lower parts of the setup were parallel to each other.GDAs were compressed from above onto the substrate samples at 1 mm/min. When 60 N threshold was achieved test was stopped for 60 s to allow viscoelastic adjustment of the GDA and the displacement corresponding with that load was maintained during this time. Again, the dwell time was chosen based more on a realistic application procedure rather than on polymer behaviour, but earlier tests showed that

Pull-off test - MSS3 2—1

Figure 6. Example of a pull-off graph of a GB sample on steel. Maximum pressure and maximum adhesion are indicated. Orange arrows pointing to the right indicate loading (increasing compression displacement), while orange arrows pointing to the left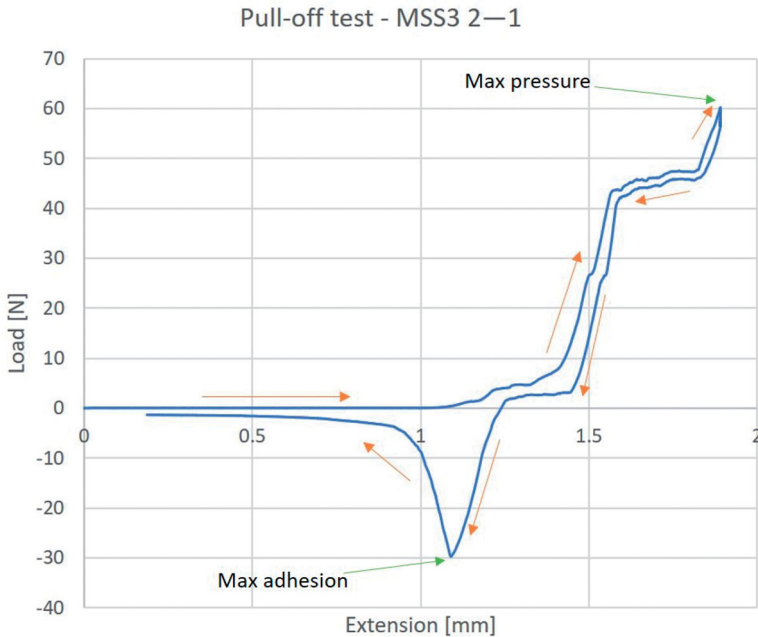 indicate unloading (decreasing compression displacement). Flat parts of the graph are a result of the viscoelastic response of the GDA and realignment of the connectors in the upper clamp of the testing setup. Since the test was set up in a way that allows certain degree of freedom to the sample (in order to maximise contact area during testing), these tolerances appear as plateaus under increasing pressure during the test.

these materials relax majority of the stress in ~5 min, with most of that happening in the first 60–90 [5]. The 60 N threshold was chosen based on the finger pressure measured in the laboratory (~15.5 N/cm^2) and later recalculated to match the area of the GDA sample. Testing speed was chosen to imitate the speed at which a delicate application of the adhesive would be conducted. However, it also allowed to assume that the PDMS stayed in its rubbery region – earlier tests conducted on very similar materials [5] with 10× higher speed showed the polymer stayed in this condition. After the relaxation stop time samples were pulled apart at 1 mm/min until they were fully separated. Adhesion was calculated from the negative load values, as shown in Figure 6. Testing was conducted on the Instron 5544 universal tested fitted with a 100 N load cell and load sensor accurate to 0.005 N (0.5% at 1/100 of the load cell capacity).

2.4. Modelling

A simplified 2D axisymmetric finite element model was developed to simulate the dry adhesive pillars tested in the pull-off experiments using Abaqus. Each simulation was used to model one 2D axisymmetric pillar to minimise the computation time. The coupling between adhesive pillars was not considered. The results

Table 1. Material properties used in the FE simulation.

Material	Young's modulus, E (GPa)	Poisson's ratio	Measured surface energy (mN/mm)	Calculated damage evolution criteria (mN/mm) UOG pillar	Calculated damage evolution criteria (mN/mm) GB pillar
Ceramic	98.6	∼0	5.143E − 5	3.895E − 5	3.923E − 5
Stainless steel 304	190	0.27	3.229E − 5	2.606E − 5	2.664E − 5
PDMS (UOG)	0.0023	0.4	1.761E − 5	N/A	N/A
PDMS (GB)	0.0011	0.29	1.933E − 5	N/A	N/A

obtained from single pillar simulations were then utilised accordingly to simulate the adhesion of the respective GDA pad samples in the experiments. This was done by modelling the pull-off force exhibited from one pillar in contact with the respective surfaces and then multiplying this result by the number of pillars on the respective GDA pads.

A model was developed for both the UOG and GB pillar in contact with a rigid flat, in order to mimic the experiments where pillars are in contact with a hard, well-polished surface. The model assumes linear elastic behaviour and the material used for both pillars was PDMS, with Young's modulus and Poisson's ratio taken from the manufacturers' datasheets, with values shown in Table 1. The pillar geometries and dimensions used to build the models were measured from ESEM images (as shown in Figure 2) of the respective pillars used in the experiments. The test procedure simulated in the FE model comprises the pillar being displaced towards the rigid flat in the normal direction before being pulled in the opposite direction in a subsequent step. This aimed to simulate the GDA substrates being forced onto the substrate surfaces before being pulled away in the pull-off tests. All bodies were fixed in the tangential direction during the FE simulations. The substrate used in the respective FE simulations was treated as an idealised rigid flat body. This meant that the FE simulation was only used to compare the respective GDA patches being separated from the lowest roughness (sub-micron) ceramic and steel surfaces.

The Rq for these substrates was suitably low to allow for a reasonable comparison to the cylindrical and mushroom tip pillars pull-off simulations. The contact interface used in the model utilises cohesive zone modelling (CZM) which aims to introduce the phenomenological law to describe the normal traction-opening displacement on the bonding interface. This model describes the adhesion energy between two surfaces and by extension the energy or work required to separate them [66]. The separation of the pillars and the substrate is governed by a damage evolution criterion. The cohesive element detachment occurs once the separation energy equals the work of adhesion. The respective values for the work of adhesion between two dissimilar surfaces can be determined as follows [67]:

$$w \approx \gamma_1 + \gamma_2 - \sqrt{\gamma_1 \gamma_2} \qquad (1)$$

This allows adhesion energy between two respective surfaces to be calculated using their respective surface energies γ_1 and γ_2. The respective surface energies of the
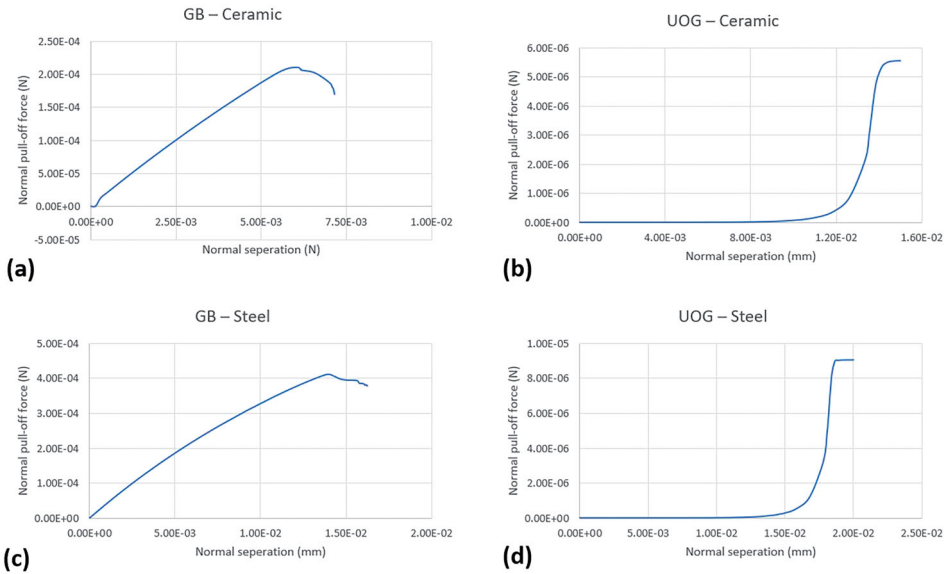
Figure 7. Normal separation vs. Pull-off force graphs for the FE models. GB pillar-ceramic interaction (a), UOG pillar-ceramic interaction (b), GB pillar-steel interaction (c), UOG pillar-steel interaction (d).

substrates and GDAs used were taken from the experimental work conducted in this research and are detailed in Table 1. The calculated adhesion energy between the two surfaces serves as the CZM detachment criteria for the separation of the interfacial elements in the FE models. Once the required energy, w, in the damage evolution criterion is reached due to the pillar being pulled away from the surface then a separation of the respective interfacial elements is allowed to occur. This allows us to measure a pull-off force associated with the pillar detachment from the substrate. The pull-off force for each simulation is measured from the pillar top surface. As demonstrated in the experimental tests as well.

Figure 7 shows the associated pull-off force for each of the FE models. These figures demonstrate the evolution of the pull-off force associated with the pillar tops, along with the evolution of the average normal separation of the pillar-substrate interface. This demonstrates the experimental action of the GDA pillars being pulled upwards and away from the substrate surface. Here we see the variation in the evolution of the pull-off load and slight change in modes of separation associated with the two different types of the pillar. These plots are further discussed in the results section. These force-displacement plots along with Figure 8 enable us to understand the detachment mechanisms associated with the two different types of GDA pads.

3. Results

The three (formerly) glazed ceramic shards, one unglazed ceramic shard and one glass shard were photographed, imaged under an optical microscope and scanned with a mechanical and an optical profilometer (Table 2 for detailed results), The average Ra
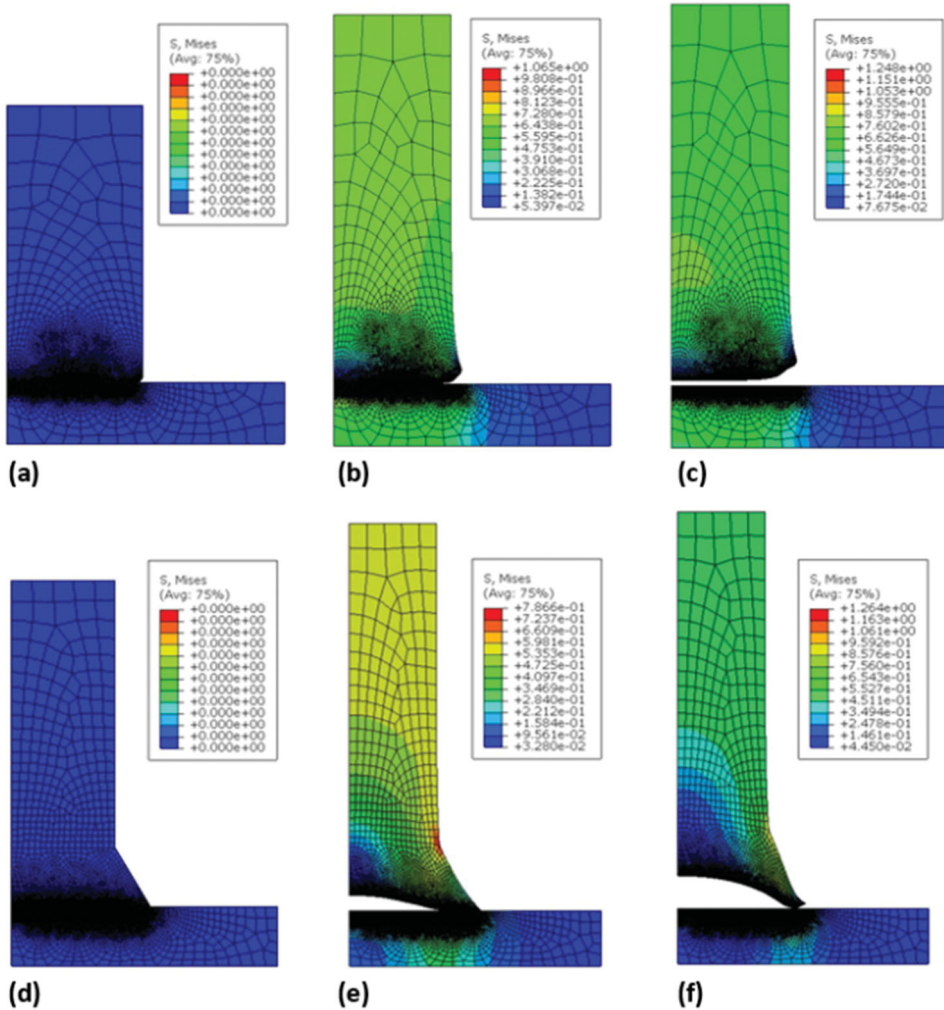
Figure 8. FE models of GB GDA (A) and UOG GDA (B). Model shows difference in crack initiation patterns, with GB detaching first in the centre and UOG detaching from the rim.

roughness ranged between $0.17 \pm 0.12\,\mu m$ and $21.33 \pm 1.99\,\mu m$ and average Rq ranged between $0.32 \pm 0.22\,\mu m$ and $26.29 \pm 2.44\,\mu m$. The average Ra roughness of the two copper coins ranged between $0.42 \pm 0.11\,\mu m$ and $4.77 \pm 1.92\,\mu m$ on its reverse (with average Rq raging between $0.58 \pm 0.16\,\mu m$ and $5.86 \pm 2.23\,\mu m$).

Overall, 5 ceramic, 7 steel and 5 PTFE samples were used in the tests. Detailed results are presented in Table 2. Average Ra roughness of ceramic samples spanned between $0.04 \pm 0.003\,\mu m$ and $4.68 \pm 0.58\,\mu m$. Steel samples spanned between $0.01 \pm 0.001\,\mu m$ and $4.07 \pm 0.37\,\mu m$. Average Ra roughness of PTFE samples ranged between $0.06 \pm 0.004\,\mu m$ and $1.54 \pm 0.007\,\mu m$. Average Rq (RMS) roughness measured in each material ranged between $0.05 \pm 0.004\,\mu m$ and $7.19 \pm 1.14\,\mu m$ for ceramics, between $0.02 \pm 0.001\,\mu m$ and $5.37 \pm 0.51\,\mu m$ for steel and between $0.08 \pm 0.006\,\mu m$ and $2.13 \pm 0.11\,\mu m\,\mu m$ in PTFE samples.

Table 2. Selected roughness parameters and surface energy of all historical reference objects and manufactured substrate samples.

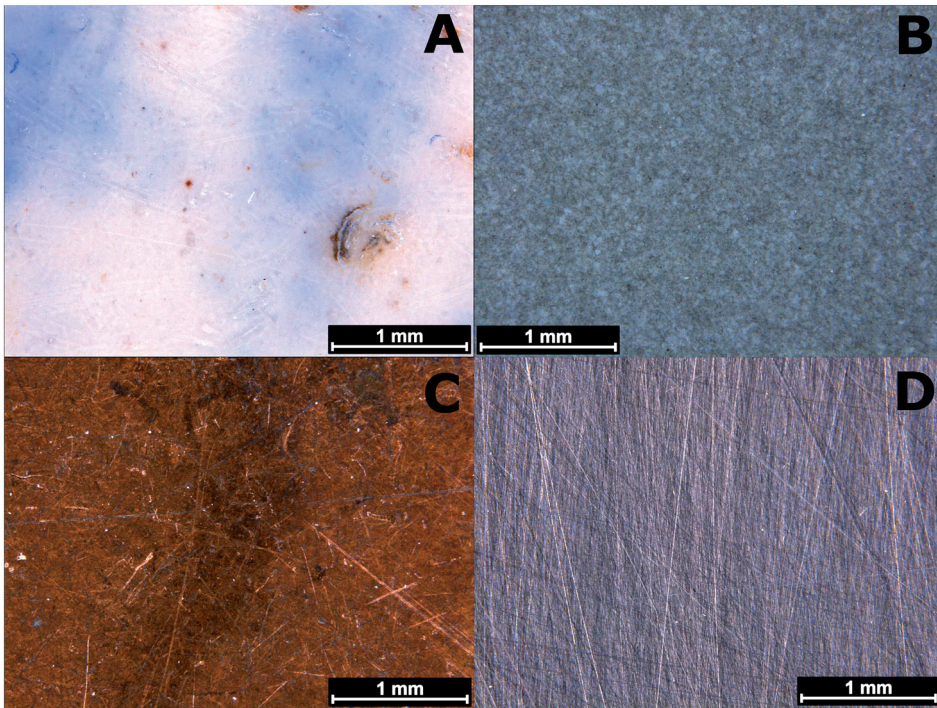|	Code	Type	Ra (μm)	Rq (μm)	Rz (μm)	Rku	Ri (μm²)	Surface Energy (mN/m)	SE-P (mN/m)	SE-D (mN/m)
Original objects	MCC1	Copper coin – Obverse	3.77	4.74	20.57	3.26	101.88			
		Copper coin – Reverse	2.32	2.92	12.93	3.11	47.90			
	MCC2	Copper coin – Obverse	4.77	5.86	26.46	3.61	161.07	29.55	5.06	24.49
		Copper coin – Reverse	7.06	8.93	38.63	3.23	304.42			
	GNE1	Glass bottle fragment, archaeological, inside	0.17	0.31	2.07	15.61	1.30	50.92	35.27	15.66
		Glass bottle fragment, archaeological, outside	7.09	9.70	46.83	5.83	544.16			
	CGE5	Ceramic plate fragment, glazed, archaeological, inside	0.55	1.54	8.50	11.66	41.14	49.67	32.74	16.94
		Ceramic plate fragment, glazed, archaeological, outside	0.64	1.03	6.75	12.88	10.74			
	CGE1	Ceramic plate fragment, glazed, archaeological, inside	4.66	6.47	40.82	9.04	335.41			
		Ceramic plate fragment, glazed, archaeological, outside	11.23	15.06	75.54	5.53	1317.91			
	CGE9	Ceramic vessel fragment, non-glazed, archaeological, inside	21.33	26.29	116.87	3.00	3257.39			
		Ceramic vessel fragment, non-glazed, archaeological, outside	21.32	25.86	111.57	2.93	3120.10			
Testing samples	CGSX	Ceramic tile	0.04	0.05	0.24	2.88	1.59	51.37	34.87	16.50
	CGS6	Ceramic tile	0.56	0.91	10.18	52.81	13.59	31.86	10.97	20.89
	CGS10	Ceramic tile	1.31	2.49	17.49	23.75	47.49			
	MSS7	Stainless steel	0.01	0.02	0.09	2.95	1.29	32.29	10.55	21.74
	MSS3	Stainless steel	0.70	0.89	5.94	3.31	16.16			
	MSS6	Stainless steel	1.07	1.36	9.14	3.33	35.94			
	MSS5	Stainless steel	2.46	3.27	20.37	5.61	112.39			
	MSS4	Stainless steel	4.07	5.37	34.65	5.66	264.17			
	PPS9	PTFE	0.06	0.076	0.443	4.460	0.10			
	PPS8	PTFE	0.66	0.83	5.37	3.16	14.92	21.93	0.01	21.92
	PPS7	PTFE	0.69	0.97	9.24	28.48	19.20			
	PPS1	PTFE	0.83	1.06	7.11	3.58	22.99			
	PPS5	PTFE	1.54	2.13	17.29	13.07	68.89			

Figure 9. Comparison between heritage objects and manufactured samples. In both heritage objects – (A, C) – deeper pitting that could not be replicated with simple polishing in test samples – (B, D) is visible. However, the density and depth of the scratches looks very similar.

Surface energy was measured on the smoothest surface available in each material, including testing substrate samples. This was done because the Ra roughness of 0.5 μm is considered to be the threshold above which surface asperities distort the contact angle and the measurements become unreliable [68]. Detailed results of these measurements are presented in Table 2. Three reference materials from the collections were characterised by the contact angle measurements: a copper penny coin, a ceramic shard, and a glass shard. The surface energy of these objects was 29.5 mN/m, 49.7 mN/m, and 50.9 mN/m respectively. The measurements were also conducted on the substrate samples. In PTFE calculated surface energy was 21.9 mN/m, in the steel sample it was 32.3 mN/m. Ceramic samples were measured in two conditions, once on a sample with intact glaze and once on a sample with the top layer of the glazed polished off. In the first case, the SE was measured to be 51.4 mN/m and in the second case, it was 31.9 mN/m. The surface energy of the polymer in the GDAs was measured to be 19.3 mN/m in GB GDAs and 17.6 mN/m in UOG GDAs. The results were comparable between new samples and heritage materials, including visual assessment (Figure 9).

The pull-off tests were conducted with each of the two GDA on the same set of substrate samples with an Instron 5544 universal tester with Bluehill 3 software and fitted with a custom-built environmental chamber. Testing was conducted at $55 \pm 3\%$ RH and $21 \pm 1\,°C$. Each GDA was represented by 6 samples, each sample was cycled through 3 attachment-detachment cycles. As a result, the presented averages come from 18 individual attachment-detachment cycles. The results are summarised in Table 3. The GB GDA

Table 3. Summary of all of the pull-off test conducted with both types of GDAs.

	Substrate	Surface roughness Ra (μm)	Adhesion Average (N)	Average per cm^2 (N/cm^2)	Standard deviation (N)	Min. (N)	Max. (N)
GB GDA							
Ceramic	CGSX	0.04	22.87	5.99	7.33	14.77	36.61
	CGS6	0.56	0.49	0.13	0.24	0.20	0.97
	CGS10	1.31	0.10	0.03	0.06	0.00	0.22
	CGS11	2.47	0.09	0.02	0.06	0.02	0.22
	CGS13	4.68	0.12	0.03	0.08	0.03	0.29
Steel	MSS7	0.01	44.92	11.76	6.30	35.48	59.34
	MSS3	0.70	21.84	5.72	6.72	7.71	30.90
	MSS6	1.07	15.51	4.06	6.51	0.00	1.73
	MSS9	1.40	0.38	0.10	0.14	0.12	0.62
	MSS10	1.95	4.22	1.11	1.33	1.95	6.20
	MSS5	2.46	3.10	0.81	1.08	1.24	4.62
	MSS4	4.07	0.77	0.20	0.52	0.05	1.82
PTFE	PPS9	0.06	13.73	3.59	4.51	5.90	22.11
	PPS8	0.66	0.70	0.18	0.50	0.15	1.79
	PPS7	0.69	0.27	0.07	0.15	0.00	0.46
	PPS1	0.83	1.24	0.33	0.63	0.30	2.47
	PPS5	1.54	0.07	0.02	0.04	0.00	0.16
UOG GDA							
Ceramic	CGSX	0.04	0.45	0.12	0.59	0.00	2.22
	CGS6	0.56	0.09	0.02	0.10	0.00	0.33
	CGS10	1.31	0.03	0.01	0.04	0.00	0.17
	CGS11	2.47	0.09	0.02	0.07	0.03	0.22
	CGS13	4.68	0.04	0.01	0.02	0.01	0.11
Steel	MSS7	0.01	0.74	0.19	0.96	0.00	2.90
	MSS3	0.70	0.77	0.20	0.88	0.00	2.65
	MSS6	1.07	0.89	0.23	1.28	0.00	4.01
	MSS9	1.40	0.11	0.03	0.04	0.06	0.19
	MSS10	1.95	0.19	0.05	0.14	0.01	0.49
	MSS5	2.46	0.35	0.09	0.47	0.00	1.43
	MSS4	4.07	0.05	0.01	0.04	0.00	0.10
PTFE	PPS9	0.06	0.22	0.06	0.21	0.06	0.63
	PPS8	0.66	0.00	0.00	0.00	0.00	0.00
	PPS7	0.69	0.00	0.00	0.00	0.00	0.00
	PPS1	0.83	0.00	0.00	0.00	0.00	0.00
	PPS5	1.54	0.00	0.00	0.00	0.00	0.00

(commercial, with mushroom caps) on ceramic tiles achieved between 0.1 and 22.9 N (averages of all detachment cycles). On steel, it reached between 0.9 and 44.9 N and on PTFE 0.1 and 13.7 N. The UOG2 GDA reached between 0.03 and 0.45 N on ceramic tiles, between 0 and 0.9 N on steel and between 0 and 0.22 N on the PTFE substrates. All these values presented were achieved on samples with an average area of 3.82 ± 0.02 cm^2.

In all materials and in both GDAs adhesion generally fell with increasing roughness of the substrate sample to which it had been attached (as can be seen in Figure 10). However, a decrease in adhesion happened in all cases at ~1.5 μm Ra, then increased slightly at a higher roughness. The two GDAs performed significantly differently, with the GB GDA achieving results an order of magnitude higher than the UOG GDA. However, the UOG GDA lost adhesion proportionally slower than the GB GDA with increasing roughness. The spread of results in the UOG GDA sample was also proportionally higher than this of the GB GDA. The results achieved by each GDA in the FE model compared with the experimental test are shown in Table 4. These results correlate well with the pull-off experiments: the UOG GDA model achieved 0.47 N on a
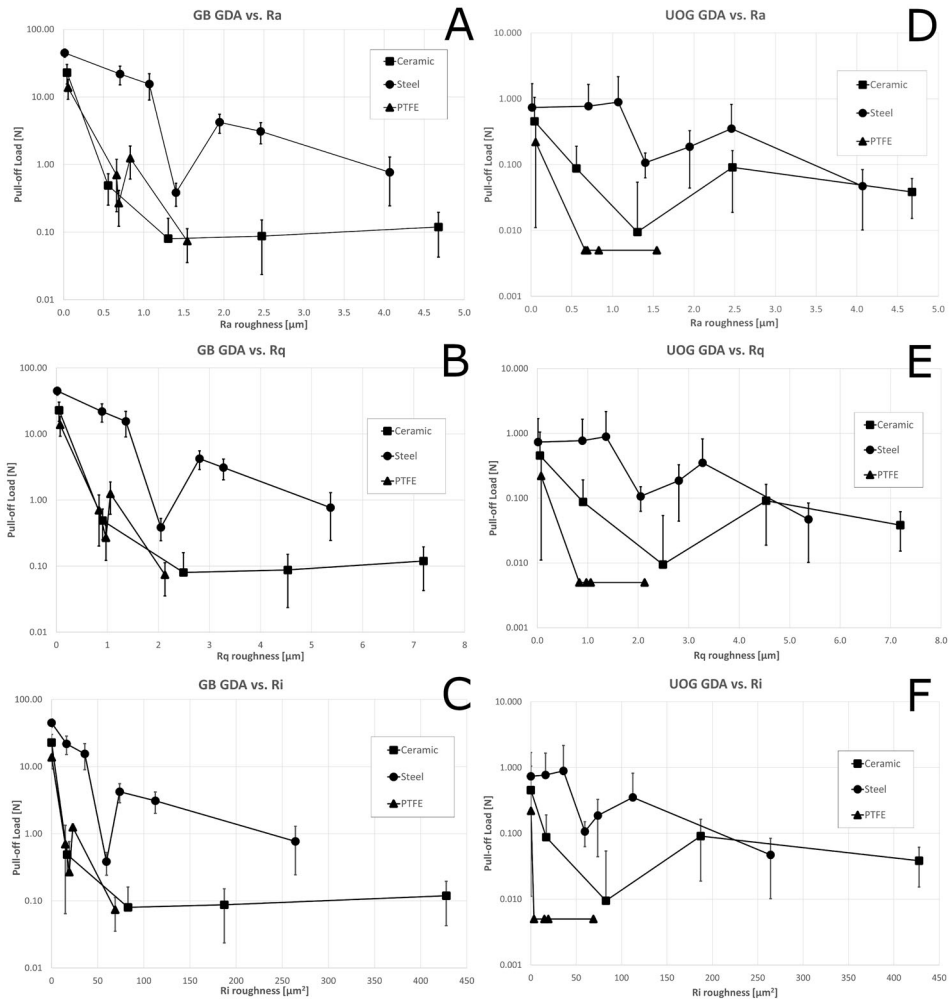
Figure 10. Graphs showing the compiled pull-off test against roughness, with GB on the left (A–C) and UOG on the right (D–F). Pull-off plotted against Ra (A, D), Rq (B, E) and Ri (C, F). Please note that the Y-axis is in base 10 log scale and the 0 N samples are marked at 0.005 N – the sensitivity threshold of the load sensor.

Table 4. Comparison of experimental pull-off tests to finite element simulation results.

	Experimental results		FE simulations	
GDA	Ceramic	Steel	Ceramic	Steel
University of Glasgow pillar	0.45 N, ±0.12 N	0.74 N, ±0.19 N	0.47 N	0.77 N
GB industrial pillar	22.87 N, ±5.99 N	44.92 N, ±11.76 N	23.01 N	45.26 N

ceramic substrate and 0.77 N on steel, and the GB GDA model reached 23.01 N on ceramic and 45.26 N on steel. This not only shows the significant difference in behaviour between the two GDAs on each substrate but also visible differences between different substrates in each material. This difference requires a micro-level explanation, hence the need for the FE model.

As the FE model results agree well with the pull-off force experimental results we can extrapolate that the mechanical behaviour exhibited in the FE model can shed light on the mechanical detachment behaviour of the GDA pillars during the tests. Figure 8 shows the mechanical behaviour of the UOG and GB pillars during three separate stages during the pull-off tests when in contact with the low Rq steel substrate. The initial relaxation of the pillar following pre-load, an intermediate step where the detachment has initiated, and finally the detachment of the pillar from the substrate. Figure 9(A–C) shows the behaviour for each of these steps for the UOG pillar, while Figure 9(D–F) shows the behaviour of the GB pillar.

The two different pillars clearly exhibit different types of mechanical detachment. The UOG pillar displays mode 1 behaviour [51]. Whereby detachment or crack propagation initiates from the outside edge of the pillar [69–72]. This relatively simple detachment mechanism results in lower pull-off forces than associated with the GB, or mushroom head pillar. The detachment mechanism is shown in Figure 9(D–F) by the GB pillar is typically termed mode 2 behaviour [51]. Where we see a more complex detachment mechanism beginning from the centre of the contact area between the pillar and the substrate. The behaviour exhibited by each pillar is extremely similar when in contact with either the low Rq steel or ceramic. Figure 7 shows the pull-off force/normal separation data for each of the FE models. This illustrates how the more complex mode of separation associated with the GB pillar results in a significantly increased pull-off force and a variation in how the average normal displacement of the interface evolves during pull-off. The data in Figure 7 highlights the very similar mechanical behaviour for the respective pillars on both the low Rq steel and ceramic substrates.

4. Discussion

The FE simulations highlight the importance of the geometry of the GDA pillar to the final adhesive strength, based on the properties of the particular substrate surface, for example, the increased roughness. The simulation showed that the mushroom head prevents separation at the outside edge of the pillar structure, resulting in a more complex detachment mechanism and a considerably larger force required to separate the GB pad from the substrates. This is consistent with previously published research on micropillar detachment [69–72]. While the GB GDA loses the adhesion quite suddenly upon the increase of surface roughness above the level of the smoothest substrate (Figure 10(A–D)), the UOG maintained a higher percentage of initial adhesive strength even with the increase in substrate roughness. This can be seen particularly well in interactions with the steel samples, where the UOG GDA has maintained consistent results until the Ra roughness increased above 1 μm. The UOG GDA also showed significant variability in adhesive strength between different patches of the same GDA. Even when an optimised Ri roughness was calculated, as proposed by Kasem and Varenberg [30], the improved fit of the data still has the overall differences (Figure 10(E–F)) between materials. It can be hypothesized that the presence of higher roughness increases the chances of creating crack initiating defects at the edges of the mushroom caps, similar to results presented by Booth et al. [71]. Rougher surfaces might also potentially also lead to increased buckling of the micropillars due to increased

difficulty to find space to retain shape under pressure. It was not possible to determine whether this situation occurs in these tests, but it is a possibility that should be considered. However, we find this unlikely as the pillars in the GDAs used to have a low aspect ratio and are on the sturdier side of possible designs. It is more likely to see the pillars being pressed into the backing layer of the material. Hence, in future tests, increased dwell time could be considered to allow for better relaxation of the polymer and adjustment of the pillars to the surface. Judging from the shapes of the graphs and the post-test examination, we concluded that the samples had very consistent elastic behaviour that they have retained after testing. The loading and unloading curves in all samples followed the same path, although slightly shifted along the displacement axis (Figure 6).

In the empirical tests both GDA types lost adhesive strength with increasing roughness earlier on the ceramic substrates than on steel. The greatest loss occurred on PTFE substrates for both GDAs and this can be explained by the very low surface energy of that surface, as the steel and ceramic substrates have both significantly higher surface energy (comparable between each other), while the PDMS has very low surface energy as well. The UOG material lost its adhesion on steel substrates proportionally slower than the UOG material, keeping the average level of adhesion on the first three samples (Figure 10). However, considering the very high spread of data for the UOG material, it can be just a statistical coincidence. The spread is probably caused by the mode of separation of the UOG flat tip pillar, which is sudden and clearly speeds up the separation of the adhesive once a crack has been initiated (Figure 7) Lack of the mushroom cap deprives the material of its mitigating effect of slower detachment. This makes flat tip material not only easier to detach but also less predictable even on seemingly smooth and flat surfaces.

Introducing the Ri improved data fit, but did not eliminate the difference completely. Since the Ra, Rq and Ri are calculated as average values of the prominence of surface features. The range is the sum of the depth of the lowest valley and the height of the highest peak in the profile. It is a parameter that is by definition very sensitive to the presence of single extreme peaks and valleys. Kurtosis of the profile is the measure of its peakedness[2], or sharpness of its surface features. It indicates how big is the part of the profile is at the tails of the spectrum. A high kurtosis value indicates that more surface features are present closer to the ends of the range, which indicates the greater presence of sharp peaks and valleys. The kurtosis (Rku) of the profile and the range (Rt) of the surface features have less influence on the final Ra and Rq values. As it can be seen from Figure 11, two profiles can have similar Ra, but profile A has a visibly lower range and kurtosis. In the case of substrate surfaces used in this research, the differences in these parameters are probably caused by their crystalline structure. Commercial ceramics have large crystals that are removed as a whole during polishing. Therefore, they leave larger and deeper pits on the surface behind them during polishing. Steel surfaces do not have this property, therefore they have a lower range of surface features – lower peaks and shallower valleys. In the case of fibrillar adhesives, which are made of polymers stiffer than other adhesives (pre-curing or non-curing), the availability of potential contact points is crucial for achieving a strong connection. As seen from the model, any gap initiating an individual crack can cause quicker
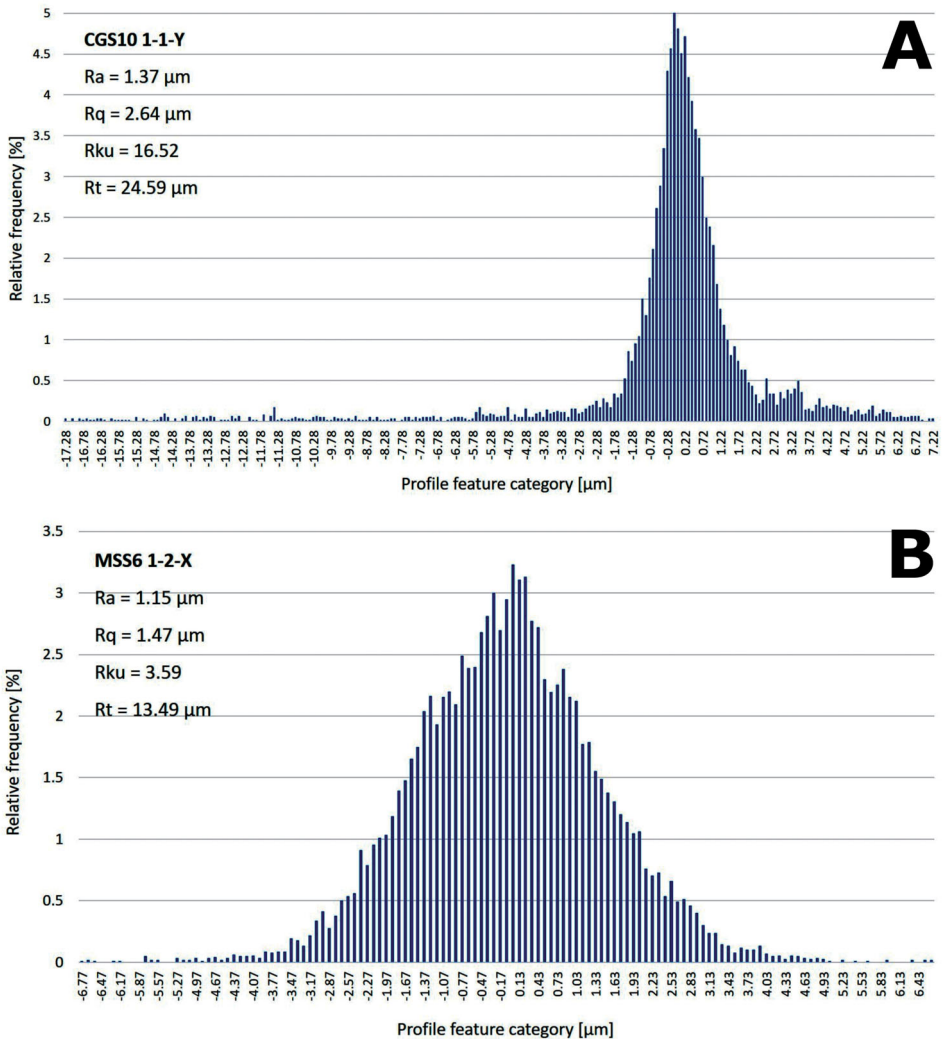
Figure 11. (A, B) Two histograms of depths of surface features – graphs showing the relative frequency of occurrence of surface features (peaks and valleys) within a given distance from the Mean Centre Line, categorized by 0.1 µm. Profiles shown have similar Ra, but very different kurtosis and range.

detachment of a micropillar. The greater the number of such events, the lower the potential adhesive strength. In most cases, GDAs have a regular distribution of the fibres of a particular length and tip area on their surfaces. Hence the greater number of pronounced surface features on the substrate necessarily reduce the potential for achieving a good connection with it. This is a crucial factor in heritage conservation, where surfaces are not standardised, and the range of potential materials, as well as the degree of their wear, can be extremely high.

Finally, a drop-in adhesive strength present in both types of GDAs at ~1.5 µm Ra roughness is most probably caused by the same tip edge crack initiating events as discussed above. Both types of GDAs in this research have pillars of similar diameter and

that is probably why they are affected in a similar manner. It can be assumed that this particular roughness has the asperities on the surface of the substrate that has a diameter similar, but somewhat smaller or larger than the diameter of the GDA micropillars. This can lead to immediate crack initiation, and it is what normally appears when the difference in size between the surface asperities and GDA micropillars is marginally larger or smaller than that of the pillars. This does not happen when the differences between these dimensions are significant [15,17]. It is worth mentioning, that plotting this data against the Ri not only does not remove this sudden drop, but it actually made it slightly steeper.

We have not investigated the influence of the surface roughness on GDA patches of different sizes and we acknowledge that this is an interesting area for further study. As the GDAs have known issues with scalability (Section 1), the measurements can be a useful reference for adhesive strength per area unit ratio, but should not be expected to linearly scale up or down. We have chosen sample sizes that should be informative and useful for potential adopters of the technology in the heritage field, but it should be noted that every use brings risks when the GDA patch deviates from the size tested here. Especially when increasing the patch area, adhesive strength per area unit can fall [5]. Additionally, it has to be acknowledged that despite creating the substitute samples that fit very well within the parameters of the original materials, factors other than roughness, surface energy and conductivity might be at play. Maybe even within these factors some parameters not taken into account (e.g. advanced roughness parameters) might influence the final results. Fibrillar adhesion is a complex phenomenon and we have done our best to isolate other potentially important factors, like changes in visco-elasticity of polymers or the occurrence of capillary phenomena. In the not reported here preliminary tests, we have seen GDAs adhering effectively underwater, but because this rarely happens in a museum setting, we have abandoned investigation of otherwise very probable [74] influence of capillary action. This is definitely a note-worthy research area with many unanswered questions.

5. Conclusions

Through this research, it has been shown how two different types of GDAs, one with a flat tip and one with a mushroom cap, behave on three different substrates with various stages of surface abrasion. The prepared samples matched the characteristics of the original cultural heritage materials closely, replicating crucial parameters of surface roughness and surface energy. The increase in roughness over time caused by the degradation of these heritage materials has been observed previously [46,47]. The staged approach with roughness increasing incrementally not only allows for tracking the GDA behaviour, but also follows the stages of material deterioration. It has been shown that the GDAs behave differently when the surface roughness of the substrate increases, but are losing adhesive strength at different rates. It is a trend, which the model helped to provide a helpful explanation: the difference in adhesive behaviour and different patterns of losing adhesive strength between the two GDAs, and the differences in the loss of adhesive strength of each GDA on different substrates upon increased roughness clearly stem from the microscale behaviour of individual pillars. It

has also been shown that different materials, despite having similar Ra roughness, can create different bond strengths with the same GDA. Therefore we suggest that the most common roughness parameters are insufficient to predict the adhesive strength loss pattern in fibrillar adhesives. Thus, more rarely reported parameters, for example, Rku is needed to explain the GDA behaviour on a particular surface. The FE model was developed to help explain the physical reasons behind the different patterns of adhesive strength loss. It has achieved very good correlation with the experimental results, adding to its robustness. The crack initiation patterns observed in the model are in agreement with published literature and they provide highly probable explanations of the micropillar behaviour. The FE model has proven to be an effective and helpful tool for explaining the adhesive behaviour of the GDAs.

This research has also shown that it is possible to successfully recreate surfaces encountered in original heritage objects for the purpose of adhesive testing. Finally, this research has shown that adapting GDAs for the field of heritage conservation will require looking beyond the most common surface roughness descriptors, as the surfaces encountered in the field have extreme variety. This work will additionally require increased knowledge in the conservation community regarding the roughness parameters and expanding a database of studied surface characteristics of heritage objects.

Notes

1. Values of the surfaces energy used: water surface energy, SE = 72.8 mN/m (polar component, SE-P = 51 mN/m and dispersive component, SE-D = 21.8 mN/m); ethylene glycol SE = 48 mN/m (SE-P = 19 mN/m, SE-D = 29 mN/m) [58]; ethanol SE = 21.4 mN/m (SE-P = 2.6 mN/m, SE-D 18.8 mN/m), xylene SE = 30.1 mN/m (SE-P = 0 mN/m, SE-D 30.1 mN/m)[59].
2. Not to be confused with 'peakedness" understood as a description of the distribution curve of the features on the histogram, of which kurtosis is not a good descriptor[73].

Acknowledgments

Disclosure statement

No potential conflict of interest was reported by the author(s).

Other materials suppliers:
Ceramic tiles – Troy Ceramic, Obtained from B & Q Hardware Store, Glasgow, UK
PTFE – Obtained from Trent Plastics, Gainsborough, UK
Steel – Obtained from Steel Express Ltd, Wolverhampton, UK

References

[1] Autumn K, Liang YA, Hsieh ST, et al. Adhesive force of a single gecko foot-hair. Nature. 2000;405(6787):681–685.
[2] Sitti M, Fearing RS. Synthetic gecko foot-hair micro/nano-structures as dry adhesives. J Adhes Sci Technol. 2003;17(8):1055–1074.

[3]   Wang L, Hui Y, Fu C, et al. Recent advances in gecko-inspired adhesive materials and application. J AdhesSci Technol. 2020;34(21):2275–2291.

[4]   Olender J. Silver bullet? Not yet. Gecko-inspired dry adhesives: perspectives on the technology and its future in conservation. Pict Restor. 2020;57:44–51.

[5]   Olender J. Gecko-inspired dry adhesives: evaluating their applicability to the conservation of cultural heritage. London (UK): Courtauld Institute of Art; 2019.

[6]   Fenn J. Adhesion without adhesives: gecko-Like adhesives. In: Adhesives and consolidants for conservation: research and applications. Ottawa (Canada): Canadian Conservation Institute; 2011.

[7]   Appelbaum B. Criteria for treatment: reversibility. J Am Inst Conserv. 1987;26(2): 65–73.

[8]   Appelbaum B. Conservation treatment methodology. Oxford (UK): Butterworth-Heinemann; 2007.

[9]   Muñoz Viñas S. Contemporary theory of conservation. Oxford (UK): Butterworth-Heinemann; 2005.

[10] Oddy WA. Does reversibility exist in conservation? In: Oddy WA, Carroll S, editors. Reversibility - does it exist? London (UK): British Museum; 1999. p. 1–5.

[11] Storari M, Lorenzo F, Cattaneo B, et al. "Vortice e Figura" Di Paola Levi Montalcini: Intervento Su u n'opera Polimaterica Con Supporti Footografici Affetti Da Sindrome Acetica. Paper presented at the XVII Congresso Nazionale IGIIC – Lo Stato dell'Arte – Chiesa di Cristo Flagellato dell'ex Ospedale San Rocco, Matera; 2019 October 10–12; Matera, Italy.

[12] Olender J, Young C, Taylor A. The applicability of gecko-inspired dry adhesives to the conservation of photographic prints. In: Bridgland J, editor. ICOM-CC 18th triennial conference preprints. Paris (France): International Council of Museums; 2017. p. 0913.

[13] Izadi H, Dogra N, Perreault F, et al. Removal of particulate contamination from solid surfaces using polymeric micropillars. ACS Appl Mater Interfaces. 2016;8(26): 16967–16978.

[14] Olender J. Możliwości zaadaptowania najnowszych osiągnięć inżynierii materiałowej Na potrzeby konserwacji dzieł sztuki. Toruń (Poland): Nicolaus Copernicus University, 2014.

[15] Huber G, Gorb SN, Hosoda N, et al. Influence of surface roughness on gecko adhesion. Acta Biomater. 2007;3(4):607–610.

[16] Davies J, Haq S, Hawke T, et al. A practical approach to the development of a synthetic gecko tape. Int J Adhes Adhes. 2009;29(4):380–390.

[17] Cañas N, Kamperman M, Völker B, et al. Effect of nano- and micro-roughness on adhesion of bioinspired micropatterned surfaces. Acta Biomater. 2012;8(1):282–288.

[18] Pillai R, Nordberg E, Riedel J, et al. Geckos cling best to, and prefer to use, rough surfaces. Front Zool. 2020;17(1):32.

[19] Li X, Tao D, Lu H, et al. Recent developments in gecko-inspired dry adhesive surfaces from fabrication to application. Surf Topogr: Metrol Prop. 2019;7(2):023001.

[20] Arzt E, Quan H, McMeeking RM, et al. Functional surface microstructures inspired by nature – from adhesion and wetting principles to sustainable new devices. Prog Mater Sci. 2021;120:100823.

[21] Basak S. Redefining stickiness–a reflection on the gecko inspired adhesives possessing self-cleaning traits. J Adhes Sci Technol. 2021;35(14):1473–1491.

[22] Niewiarowski PH, Stark AY, Dhinojwala A. Sticking to the story: outstanding challenges in gecko-inspired adhesives. J Exp Biol. 2016;219(7):912–919.

[23] Sahay R, Baji A, Ranganath AS, et al. Durable adhesives based on electrospun poly(vinylidene fluoride) fibers. J Appl Polym Sci. 2017;134(2):1–7.

[24] Barreau V, Hensel R, Guimard NK, et al. Fibrillar elastomeric micropatterns create tunable adhesion even to rough surfaces. Adv Funct Mater. 2016;26(26):4687–4694.

[25] Das S, Cadirov N, Chary S, et al. Stick-slip friction of gecko-mimetic flaps on smooth and rough surfaces. J R Soc Interface. 2015;12(104):20141346.

[26]   Ruffatto D, Parness A, Spenko M. Improving controllable adhesion on both rough and smooth surfaces with a hybrid electrostatic/gecko-like adhesive. J R Soc Interface. 2014; 11(93):20131089.

[27]   Xue L, Pham JT, Iturri J, et al. Stick-slip friction of PDMS surfaces for bioinspired adhesives. Langmuir. 2016;32(10):2428–2435.

[28]   Dening K, Heepe L, Afferrante L, et al. Adhesion control by inflation: implications from biology to artificial attachment device. Appl Phys A. 2014;116(2):567–573.

[29]   Fischer SCL, Boyadzhieva S, Hensel R, et al. Adhesion and relaxation of a soft elastomer on surfaces with skin like roughness. J Mech Behav Biomed Mater. 2018;80: 303–310.

[30]   Kasem H, Varenberg M. Effect of counterface roughness on adhesion of mushroom-shaped microstructure. J R Soc Interface. 2013;10(87):20130620.

[31]   Tian H, Li X, Shao J, et al. Gecko-effect inspired soft gripper with high and switchable adhesion for rough surfaces. Adv Mater Interfaces. 2019;6(18):1900875.

[32]   Tan D, Wang X, Liu Q, et al. Switchable adhesion of micropillar adhesive on rough surfaces. Small. 2019;15(50):1904248.

[33]   Tamelier J, Chary S, Turner KL. Importance of loading and unloading procedures for gecko-inspired controllable adhesives. Langmuir. 2013;29(34):10881–10890.

[34]   Tinnemann V, Hernández L, Fischer SCL, et al. In situ observation reveals local detachment mechanisms and suction effects in micropatterned adhesives. Adv Funct Mater. 2019;29(14):1807713.

[35]   Webb M. Reconstruction and natural aging of seventeenth- through nineteenth-century European lacquer formulations. Stud Conserv. 2019;64(1):S197–S212.

[36]   Costello SD, Rayner G, Eremin K. The degradation of cadmium orange restoration paint on an ancient greek terracotta vase. In: Bridgland J, editor. ICOM-CC 18th Triennial Conference Preprints. Paris (France): International Council of Museums; 2017. p. 0401.

[37]   Wong L, Han L, Chen Q, et al. Developing new approaches to the conservation of Qing dynasty painted architectural decoration at Shuxiang temple, Chengde. In: Bridgland J, editor. ICOM committee for conservation, 15th triennial conference. New Delhi (India): Allied Publishers Pvt. Ltd.; 2008. p. 938–945.

[38]   Strandberg H, Johansson L-G, Rosvall J. Outdoor bronze sculptures—a conservation view on the examination of the state of preservation. In: Bridgland J, editor. ICOM committee for conservation, 11th triennial meeting. London (UK): James and James (Science Publishers); 1996. p. 894–900.

[39]   Townsend JH, von Aderkas N, Ormsby B, et al. Kurt Schwitters' British sculptures: materials analysis and assessment of stability. In: ICOM-CC 17th triennial conference. Paris (France): International Council of Museums; 2014. p. 1011.

[40]   Langlois J, Mary G, Bluzat H, et al. Analysis and conservation of modern modeling materials found in Auguste Rodin's sculptures. Stud Conserv. 2017;62(5):247–265.

[41]   Ravines P, Wichern CM, Chen J-J. Optical and surface metrology to study cultural heritage: confocal topometry applied to the surface study of photographic images. Paper presented at the 9th International Conference on NDT of Art, Jerusalem Israel; 2008 May 25–30; Jerusalem.

[42]   Wei W. Surface micro-roughness, cleaning, and perception. In: Bridgland J, editor. ICOM-CC 16th triennial conference. Almada (Portugal): Criteiro; 2011.

[43]   Carvalhão M, Dionísio A. Evaluation of mechanical soft-abrasive blasting and chemical cleaning methods on alkyd-paint graffiti made on calcareous stones. J Cult Herit. 2015; 16(4):579–590.

[44]   Daly C. Preliminary results from a legacy indicator tool for measuring climate change related impacts on built heritage. Herit Sci. 2019;7(1):32.

[45]   Delaney JK, de la Rie ER, Elias M, et al. The role of varnishes in modifying light reflection from rough surfaces: a study of changes in light scattering caused by variations in

varnish topography and development of a drying model. Stud Conserv. 2008;53(3): 170–186.

[46] Grissom CA, Charola AE, Wachowiak MJ. Measuring surface roughness on stone: back to basics. Stud Conserv. 2000;45(2):73–84.

[47] Raneri S, Crezzini J, Arrighi S, et al. Measuring weathering and nanoparticle coating impact on surface roughness of natural stones. Stud Conserv. 2019;64(5):298–309.

[48] Fermo P, Cappelletti G, Cozzi N, et al. Hydrophobizing coatings for cultural heritage. A detailed study of resin/stone surface interaction. Appl Phys A. 2014;116(1):341–348.

[49] Ali M, Ali M, Darwish S, et al. Solvent cleaning of Antique chromogenic prints: an analytical comparative study. Mediterr Archeol Archeometry. 2017;17(3):1–12.

[50] Ciortan IM, Marchioro G, Daffara C, et al. Aging prediction of cultural heritage samples based on surface microgeometry. In: Sablatnig R, Wimmer M, editors. EUROGRAPHICS workshop on graphics and cultural heritage. Geneve (Switzerland): The Eurographics Association; 2018.

[51] Carbone G, Pierro E. Sticky bio-inspired micropillars: finding the best shape. Small. 2012;8(9):1449–1454.

[52] Carbone G, Pierro E, Gorb SN. Origin of the superior adhesive performance of mushroom-shaped microstructured surfaces. Soft Matter. 2011;7(12):5545.

[53] Carbone G, Pierro E. A review of adhesion mechanisms of mushroom-shaped microstructured adhesives. Meccanica. 2013;48(8):1819–1833.

[54] Sauer RA. Advances in the computational modeling of the gecko adhesion mechanism. J Adhes Sci Technol. 2014;28(3–4):240–255.

[55] Li G, Chang T. Effect of head shape on the adhesion capability of mushroom-like biological adhesive structures. Acta Mech Solida Sin. 2011;24(4):318–325.

[56] Kim Y, Yang C, Kim Y, et al. Designing an adhesive pillar shape with deep learning-based optimization. ACS Appl Mater Interfaces. 2020;12(21):24458–24465.

[57] ISO 19403-2. Paints and varnishes—wettability; part 2: determination of the surface free energy of solid surfaces by measuring the contact angle. London (UK): The British Standards Institution; 2020.

[58] Schuster JM, Schvezov CE, Rosenberger MR. Analysis of the results of surface free energy measurement of Ti6Al4V by different methods. Procedia Mater Sci. 2015;8: 732–741.

[59] van Oss CJ. Interfacial forces in aqueous media. 2nd ed. Boca Raton (FL): CRC Press; 2006.

[60] Rumens CV, Ziai MA, Belsey KE, et al. Swelling of PDMS networks in solvent vapours; applications for passive RFID wireless sensors. J Mater Chem C. 2015;3(39): 10091–10098.

[61] Bugnara M. Contact angle plugin for ImageJ [Internet] [cited 2020 August 15]. Available from: https://imagej.nih.gov/ij/plugins/contact-angle.html.

[62] Lamour G, Hamraoui A, Buvailo A, et al. Contact angle measurements using a simplified experimental setup. J Chem Educ. 2010;87(12):1403–1407.

[63] Owens DK, Wendt RC. Estimation of the surface free energy of polymers. J Appl Polym Sci. 1969;13(8):1741–1747.

[64] Kaelble DH. Dispersion-polar surface tension properties of organic solids. J Adhes. 1970;2(2):66–81.

[65] Röhrig M. Fabrication and analysis of bio-inspired smart surfaces. Karlsruhe (Germany): KIT Scientific Publishing; 2013.

[66] Dassault. ABAQUS/standard user's manual. Version 6.14. Providence (RI): Dassault Systemes Corp.; 2014.

[67] Mangipudi VS, Huang E, Tirrell M, et al. Measurement of interfacial adhesion between glassy polymers using the JKR method. Macromol Symp. 1996;102(1):131–143.

[68] Rudawska A, Jacniacka E. Analysis for determining surface free energy uncertainty by the Owen–Wendt method. Int J Adhes Adhes. 2009;29(4):451–457.

[69]   Hensel R, Moh K, Arzt E. Engineering micropatterned dry adhesives – from contact theory to handling applications. Adv Funct Mater. 2018;28(28):1800865.

[70]   Hensel R, McMeeking RM, Kossa A. Adhesion of a rigid punch to a confined elastic layer revisited. J Adhes. 2019;95(1):44–63.

[71]   Booth JA, Tinnemann V, Hensel R, et al. Statistical properties of defect-dependent detachment strength in bioinspired dry adhesives. J R Soc Interface. 2019;16(156): 20190239.

[72]   Fischer SCL, Arzt E, Hensel R. Composite pillars with a tunable interface for adhesion to rough substrates. ACS Appl Mater Interfaces. 2017;9(1):1036–1044.

[73]   Westfall PH. Kurtosis as peakedness, 1905 – 2014. R.I.P. Am Stat. 2014;68(3):191–195.

[74]   Stark AY, Klittich MR, Sitti M, et al. The effect of temperature and humidity on adhesion of a Gecko-Inspired adhesive: implications for the natural system. Sci Rep. 2016;6: 30936.